Tunable Highly Birefringent Bandgap-Guiding Liquid-Crystal Microstructured Fibers

Dimitrios C. Zografopoulos, Emmanouil E. Kriezis, *Member, IEEE*, and Theodoros D. Tsiboukis, *Senior Member, IEEE*

***Abstract*—A new type of nematic liquid-crystal infiltrated photonic bandgap-guiding fiber for single polarization or high-birefringence guidance is proposed. Numerical studies demonstrate that modal birefringence can be tuned by proper selection of the structural and material parameters as well as by the application of an external electric field in conjunction with the specific liquid-crystal anchoring conditions.**

***Index Terms*—Highly birefringent (HB) fibers, nematic liquid crystals (LCs), photonic crystal fibers, polarization-maintaining (PM) fibers.**

I. Introduction

MICROSTRUCTURED fibers (MFs) have attracted particular attention in the past few years, since they exhibit remarkable properties, which can be directly exploited in a wide range of modern applications, such as in spectroscopy, sensing, or in telecommunication systems [1]–[3]. Light confinement in such fibers is achieved either by a modified form of total internal reflection (mTIR) or due to the photonic bandgap effect in a low-index core, which is surrounded by a periodic cladding structure. Among other uses, MFs have been suggested as promising candidates for the design of polarization-maintaining (PM) [4], [5] and highly birefringent (HB) [6] fibers, owing to their large index contrast and their elaborate fabrication process, which allows for sophisticated microstructural design. In principle, the anisotropy needed to generate the birefringent behavior is usually induced by applying stress in the core region (form birefringence) [7] or by disturbing the symmetry of the fiber's structure (geometrical birefringence) through proper design [8], [9] or the selective addition of extra materials [10]. The utilization of PM or HB fibers may be in certain cases indispensable, since they can eliminate the influence of polarization crosstalk and mode dispersion, thus stabilizing the operation of optical devices, transmission systems or fiber lasers [11], or even provide extra-tuning capabilities, which can be exploited in phenomena such as supercontinuum generation for optical metrology, sensor technology, and optical tomography applications [12], [13].

Manuscript received March 17, 2006; revised May 21, 2006. This work was supported by the Greek General Secretariat of Research and Technology under Grant PENED/03ED936.

The authors are with the Applied and Computational Electromagnetics Laboratory, Department of Electrical and Computer Engineering, Aristotle University of Thessaloniki, 54124 Thessaloniki, Greece (e-mail: dzogra@auth.gr; mkriezis@auth.gr; tsibukis@auth.gr).

Digital Object Identifier 10.1109/JLT.2006.878495

In the present paper, we investigate numerically an alternative way toward the design of PM/HB photonic bandgap fibers. Modal birefringence can be induced by disturbing neither the fiber's structural symmetry nor the guiding defect-core region, via the infiltration of the cladding's holes with an inherently anisotropic material and, more specifically, a nematic liquid crystal (LC). The response of nematic materials to external fields or thermal variations leads to tunable properties whose exploitation in microstructured fibers has already been examined [14], [15]. In a recent study [16], we proposed the design of a PM/HB-microstructured fiber, where light was guided by mTIR through a defect core infiltrated with a nematic LC. In contrast, for the fibers investigated here guidance is achieved by the bandgap effect, while the guiding core remains hollow and, therefore, unaffected by any losses or material dispersion originating from the LC material. It is demonstrated that by appropriate design, such bandgap fibers can function both in PM and HB operation. Furthermore, the impact of the nematic director configuration on the values of modal birefringence is carefully examined, suggesting the possibility of tunable birefringence operation.

II. PM / High-Birefringence Operation

A. Structural Parameters and Layout

The proposed fiber structure follows that of a conventional two-ring honeycomb lattice photonic bandgap fiber whose cladding holes have been infiltrated with a nematic material characterized by ordinary and extraordinary indexes n_{o} and n_{e}, respectively (Fig. 1). The defect capillary in the core region is assumed to be empty $(n_{\mathrm{c}} = 1)$. The hole-to-hole distance (lattice spacing) equals Λ, the lattice-hole radius r, and the central defect-guiding core radius r_{c}. Selective filling of microstructured fibers with liquid or liquid-crystalline materials has already been demonstrated in relevant literature [17]. Arc-fusion techniques have been successfully implemented for the infiltration of central defect cores [18], while extensive control in the infiltration process of either core or cladding capillaries can be achieved by using UV curable polymers and by exploiting the difference in the infusion length among capillaries with different radii [19]. The fiber is placed between two pairs of electrodes allowing for the arbitrary control of the alignment of the LC director via an external voltage, as schematically shown in Fig. 1. Other layouts, such as those described in [15] and [20], might be more applicable and could ensure better field uniformity over the fiber's cross section.

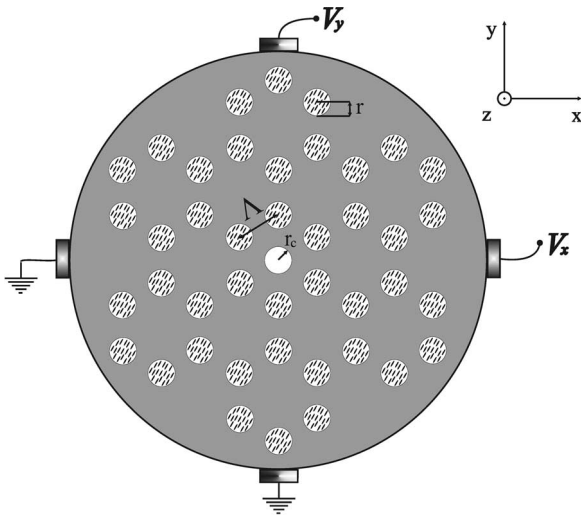

Fig. 1. Cross-sectional view of the proposed honeycomb photonic bandgap fiber: Hole-to-hole spacing Λ, lattice-hole radius r, and central defect-core radius r_c. The lattice holes have been infiltrated with a nematic LC material, while the fiber is placed between two pairs of electrodes, allowing for the arbitrary control of the nematic director. Light is guided in the central defect core, which is defined by an extra air hole.

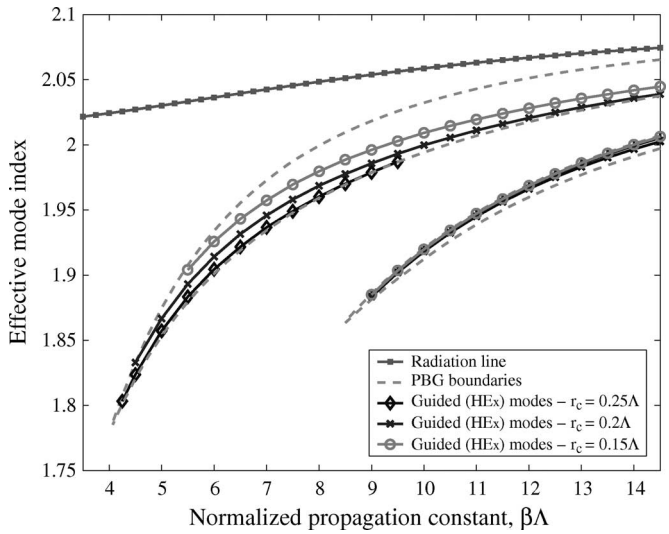

Fig. 2. Radiation line, bandgaps, and guided modes for the fiber shown in Fig. 1 in the case of y-aligned nematic LC molecules ($V_x = 0$, $V_y = V_0$). Results correspond to the following set of parameters: $n_g = 2.1$, $n_o = 1.5624$, and $n_e = 2.0904$. The fiber supports only x-polarized modes and thus operates in a PM state. For $\beta\Lambda < 9$, the fiber operates in a single-mode PM state. The cladding hole radius is kept constant at $r = 0.25\Lambda$.

For the purposes of numerical simulations, we have considered a tellurite fiberglass whose refractive index equals $n_g = 2.1$. Although tellurite fiberglass has already been proposed for the fabrication of microstructured fibers [21], [22], this particular selection serves rather indicative purposes. In principle, the only prerequisite concerning the selection of the materials used is that the fiberglass index has to be higher than the extraordinary refractive index of the nematic LC material, as it will be clarified in the analysis hereafter. Thus, there is an abundance of available material combinations, since nematic LCs with $1.5 < n_e < 2.0$ and nonsilica glasses with indexes up to $n_g = 2.2$ can be potentially used [23], [24].

All numerical calculations regarding the radiation lines and the out-of-plane bandgaps exhibited by the periodic cladding have been performed via a freely available [25] planewave expansion method [26], which solves for the eigenmodes of Maxwell's equations in periodic structures by a preconditioned conjugate-gradient minimization of the block Rayleigh quotient in a planewave basis. The dispersive characteristics of the guided modes have been calculated by a proper variation of the compact finite-difference time-domain method, which is capable of dealing with waveguiding problems where anisotropic materials are involved [27].

B. Single-Polarization Guidance

As a first example, we consider an HB isothiocyanato-based nematic compound, characterized by $n_o = 1.5624$, $n_e = 2.0904$ [28], filling the cladding's holes. We concentrate on the case where under the application of an appropriate voltage ($V_x = 0$, $V_y = V_0$), the LC director obtains a uniform pattern with all molecules lying parallel to the y-axis. As a consequence, light of x- or y-polarization should sense a different effective cladding whose air holes are filled with an isotropic material with indices equal to n_o and n_e, respectively. This diversification influences directly the out-of-plane bandgaps exhibited by the effective cladding structures, and therefore, the possibility of light guidance in the fiber's core due to the bandgap effect. For the y-polarization case, the index contrast between the fiberglass background and the cladding holes n_g/n_e is particularly low to allow for the exhibition of full bandgaps. Numerical results showed that neither bandgaps nor guided modes emerge for the frequency range studied ($\beta\Lambda < 15$, β being the propagation constant). Furthermore, n_e remains lower than the background index n_g, thus eliminating the possibility of index guiding through the LC-filled capillaries. On the contrary, the effective cladding corresponding to the x-polarization, which shows a higher index contrast (n_g/n_o), was found to support full out-of-plane bandgaps and accordingly propagating modes (Fig. 2). The dispersion curve of the fundamental x-polarized guided mode can be finely adjusted by varying the central defect-core radius. Smaller defect-core radii tend to raise the effective index of the guided modes due to the concentration of more energy in the dielectric. At $\beta\Lambda = 9$, higher order modes emerge, thus indicating the limit for single-mode operation. In case the LC molecules are aligned with the x-axis ($V_x = V_0$, $V_y = 0$), the above analysis is still valid, yet the fiber allows for the propagation of the y-polarized modes only. Conclusively, for the frequency regime $4 < \beta\Lambda < 9$, the fiber was demonstrated to operate in a selective single-mode/PM state, where the allowed polarization can be controlled by the application of the external voltage.

C. High-Birefringence Guidance

For the purpose of examining the possibility of high-birefringence operation, we studied the impact of infiltrating the cladding holes with a common nematic LC material such as the compound E7, which is characterized by $n_o = 1.5024$ and $n_e = 1.697$ at 25 °C and $\lambda = 1$ μm [29]. We consider again the uniform case that involves a y-aligned nematic director.

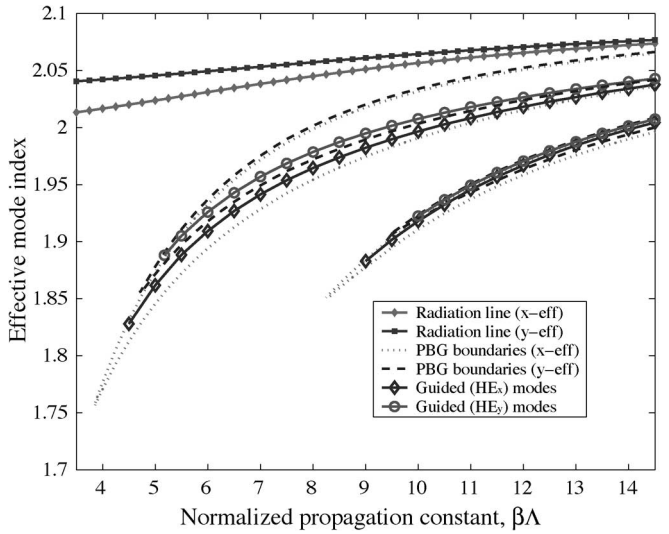

Fig. 3. Radiation line, bandgaps, and guided modes for the fiber shown in Fig. 1, in the case of y-aligned nematic LC molecules ($V_x = 0$, $V_y = V_0$). Results correspond to the following set of parameters: $n_g = 2.1$, $n_o = 1.5024$, $n_e = 1.697$, $r_c = 0.2\Lambda$, and $r = 0.25\Lambda$. The fiber supports modes of both polarizations with different effective indices and thus operates in a high-birefringence state. For $5.5 < \beta\Lambda < 8.5$, the fiber operates in a single-mode high-birefringence state.

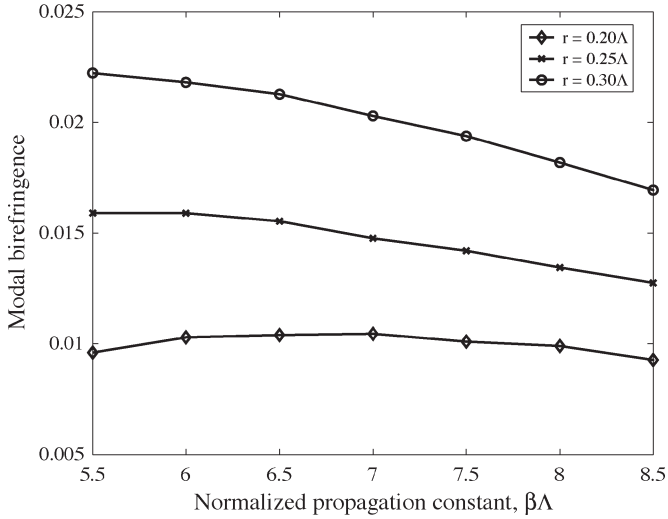

Fig. 4. Modal birefringence in the single-mode operation regime for different values of the lattice-hole radius r for the fiber studied in Fig. 3. The defect-core radius is kept constant at $r_c = 0.2\Lambda$.

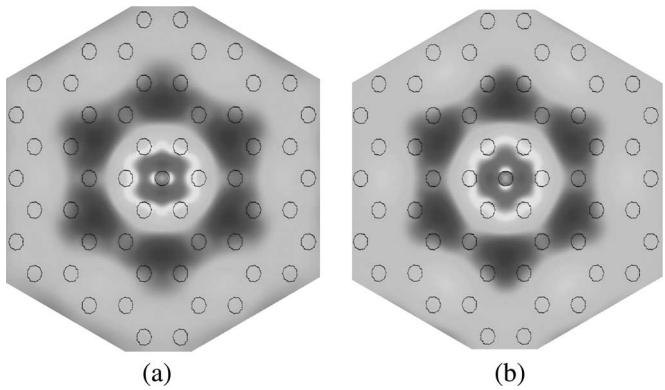

Fig. 5. Modal intensity profiles at $\beta\Lambda = 7$ for (a) the x-polarized and (b) the y-polarized fundamental mode of the fiber studied in Fig. 3. Since the core-guiding region is not infiltrated, both modes exhibit a similar profile.

The index contrast between the LC refractive indices and the glass background is now comparable for light of either x- or y-polarization, permitting the existence of full transversal out-of-plane bandgaps within a common frequency range. The results presented in Fig. 3 demonstrate that in this case, the bandgap fiber is capable of guiding light of both polarizations, yet with different dispersive properties due to the induced anisotropy of the cladding. The guided modes fit accurately within the reference bandgaps calculated for the two limiting effective isotropic claddings, which is for n_g/n_o and n_g/n_e. For the frequency range $5.5 < \beta\Lambda < 8.5$, no higher order modes appear, and the fiber remains within a single-mode operational regime. The values of the modal birefringence can be significantly adjusted by properly selecting the radius of the cladding holes. Larger holes imply the infiltration of extensive anisotropic nematic LC material, thus leading to higher values of the birefringence, as shown in Fig. 4.

For $r = 0.3\Lambda$, values higher than 0.02 can be achieved almost in the entire single-mode regime. Finally, Fig. 5 shows the modal-intensity profiles for the fundamental x- and y-polarized modes at $\beta\Lambda = 7$. It is interesting to note that the infiltrated cladding does not affect the guiding core, hence the similarity in the profiles for both polarizations of the fundamental mode. While the modal profiles of Fig. 5 indicate that the fundamental mode is LP_{01}-like, simulations have shown that higher order modes, which are guided within the second bandgap region, are LP_{11}-like. In both cases, light confinement is degraded as the modal effective index obtains values closer to the bandgap edges, due to coupling with radiating cladding modes.

D. Impact of the Nematic Director Pattern

In the analysis, so far, we have considered the case where the application of a sufficiently high-external electric field forces the LC molecules to align with the y- or x-axis, leading to a uniform director pattern. In a generalized approach, the director distribution of a nematic material confined in closed capillary cavities is determined by an interplay among the physics of elastic theory, the anchoring conditions at the cavity's surface, and the impact of any external fields. Fig. 6 shows two theoretically predicted and experimentally observed common profiles under homeotropic (perpendicular) anchoring conditions, i.e., the planar-polar (PP) and the escaped-radial (ER) profiles. In the absence of external fields, the PP texture can be analytically calculated under the one elastic constant approximation ($K_{11} = K_{33} = K$) by minimizing the elastic free energy of the LC molecules in the capillary [30]. In polar coordinates, the PP pattern is given by

$$\psi(r,\phi) = \frac{\pi}{2} - \tan^{-1}\left[\frac{(R^2+\gamma r^2)}{(R^2-\gamma r^2)}\tan\phi\right] \qquad (1)$$

where ψ is the angle between the director and the radial unit vector, R is the radius of the capillary, $\gamma = (\xi^2+1)^{1/2} - \xi$, $\xi = 2K/RW_0$, RW_0/K is the effective anchoring strength,

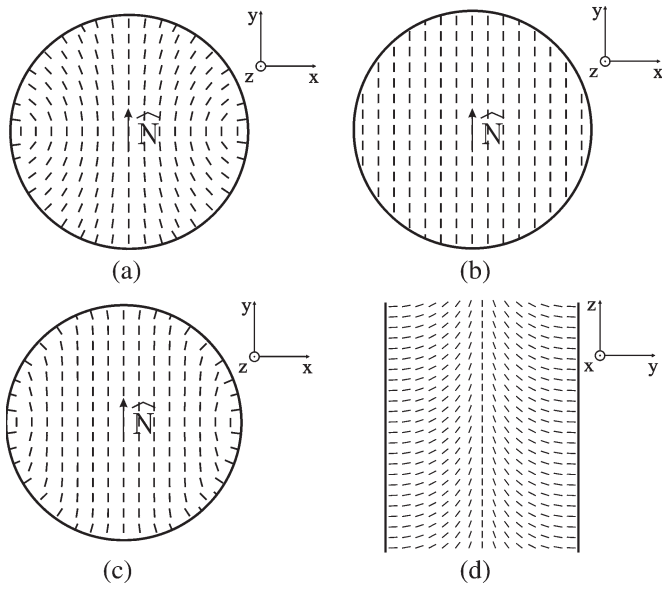

Fig. 6. Commonly observed nematic liquid-crystal director configurations (a) PP profile at the strong-anchoring limit ($\xi \to 0$) in the absence of an external field ($\xi' \to \infty$). (b) PP profile at the weak-anchoring limit ($\xi \to \infty$) in the absence of an external field ($\xi' \to \infty$). (c) PP profile at the strong anchoring ($\xi \to 0$) under strong external field ($\xi' \to 0$) limit. (d) ER profile at the strong-anchoring limit ($\sigma \to \infty$) in the absence of an external field.

which determines the orientation of the molecules at the cavity wall. Phase-transition diagrams in [31] show that for $K_{11} = K_{33}$, the PP pattern is very likely to be observed for homeotropic anchoring conditions and for small radii. A principal pattern-axis $\hat{N}$ should also be defined, expressing the average direction that characterizes the material orientation over the complete cross section of the capillary (the y-axis, for instance, in Fig. 6).

In the presence of an external field, an analytical expression for the PP profile may no longer be available. The director pattern under the one-constant approximation is then calculated [32] from the following partial differential equation (expressed in a cylindrical coordinate system):

$$\nabla^2 \theta_n - \frac{1}{\xi'^2} \cos\theta_n \sin\theta_n = 0 \tag{2}$$

where θ_n is the angle between the pattern axis and the director. Assuming an external electric (either than magnetic) field, ξ' is defined by

$$\xi' = \left| \frac{K}{\Delta\epsilon\epsilon_0} \right|^{1/2} \frac{1}{E} \tag{3}$$

K being the elastic constant and $\Delta\epsilon$ the static anisotropy of the liquid-crystalline dielectric constant, which for the nematic material E7, obtain the values $K = 10.3$ pN and $\Delta\epsilon = 13.3$ [33]. Equation (2) can be numerically solved using an iterative successive overrelaxation scheme. A typical PP pattern at the strong homeotropic anchoring limit for a high-intensity electric field is shown in Fig. 6(c).

In the case of the ER pattern, the director remains radial on the transverse plane close to the cavity wall, yet escapes in the third dimension while moving toward the cylinder axis. The ER director profile in polar coordinates is given by

$$\psi(r, \phi) = 0 \tag{4}$$

$$\theta(r) = \frac{\pi}{2} - 2\tan^{-1}\left(\frac{r}{R}\tan(a/2)\right) \tag{5}$$

with ψ interpreted as in (1), θ being the angle between the director and the xy-plane, $a = \pi/2 - \theta(r = R) = \cos^{-1}(1/\sigma)$, and $\sigma = RW_0/K + K_{24}/K - 1$ is the parameter that expresses the anchoring strength, which is considered to be larger than unity. In the case of strong anchoring ($\sigma \to \infty$), the molecules are perpendicularly aligned to the cavity wall [Fig. 6(d)]; while moving toward the weak-anchoring limit ($\sigma = 1$), the molecules obtain a uniform alignment parallel to the z-axis. For cylindrical cavities of small radii ($r \leq 0.4$ μm), the PP texture is in general promoted, while for larger radii, the ER pattern is more likely to be observed [33]. In the case of the bandgap fiber studied, a set of typical values such as $\beta\Lambda \approx 7$, $n_{\text{eff}} \approx 1.95$, and $r = 0.25\Lambda$ will result in a value of $r \approx 215$ nm for the cladding hole radius at an operational wavelength of 1500 nm, suggesting that the PP pattern will be more probably encountered in practice.

In the context of the present study, it is expected that the infiltration of the proposed bandgap fibers with a nematic material that exhibits the ER profile would offer no possibility for inducing any birefringent phenomena due to the pattern's radial symmetry. Both polarizations would sense a similar effective cladding, allowing for the emergence of degenerated propagating modes only. On the other hand, the PP texture lacks such symmetry, and it is expected to induce modal birefringence. While moving away from the weak-anchoring limit (uniform profile), the birefringent behavior should be degraded, since the uniform profile offers the maximum difference (equal to $\Delta n = n_{\text{e}} - n_{\text{o}}$) for the hole indices of the effective claddings corresponding to x- and y-polarized light.

Numerical simulations prove the above reasoning. The dispersive properties of the PM and HB fibers presented in Sections II-B and C were examined, assuming the PP profile for the infiltrated nematic material for different values of the parameter ξ under the assumption that all principal pattern axes are oriented along the y-axis. Such an alignment of the principal axes over all capillaries of the cladding might be primarily induced by applying a high-voltage pulse and then by maintaining the desired orientation using a low holding-voltage without necessarily unfolding the PP pattern. In addition, it is possible to memorize or promote a particular principal pattern-axis orientation at the filling stage by subjecting the LC material to an external field of appropriate strength and direction. For the single-polarization case, the fiber remained PM, yet the dispersion curve of the fundamental guided mode shifted, obtaining higher values (Fig. 7). While moving toward the strong-anchoring limit ($\xi = 0$), the x-polarization senses an effective index in the cladding holes, which is higher than n_{o}, and consequently, the dispersion curve is also raised. The effect of the anchoring conditions is more apparent in the case of the HB fiber, where modal birefringence is substantially influenced by the anchoring strength, as evidenced by Fig. 8. In the case of

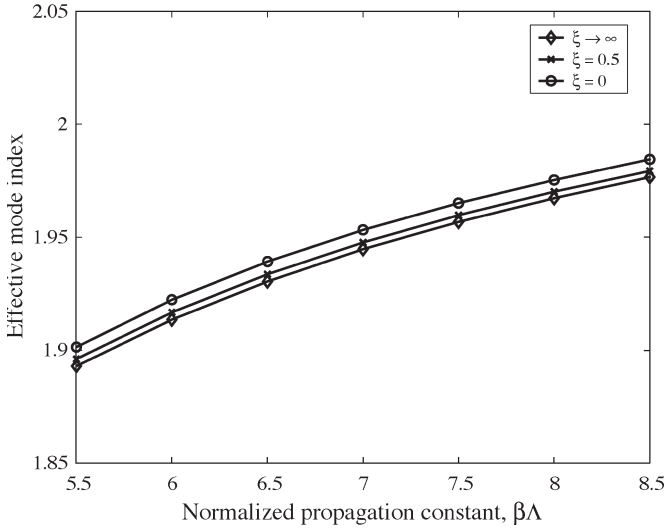

Fig. 7. Impact of the anchoring strength on the dispersive properties of the PM bandgap fiber studied in Fig. 2 for a PP configuration of the nematic material infiltrated in the lattice holes. The defect-core radius is kept at $r_c = 0.2\Lambda$ and the cladding hole radius at $r = 0.25\Lambda$.

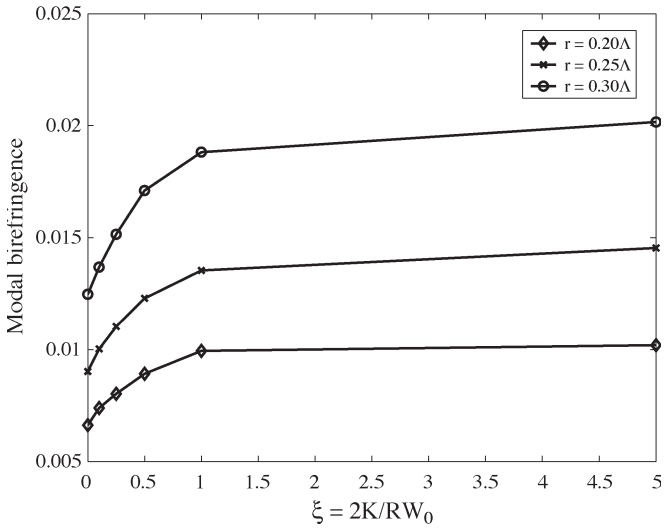

Fig. 8. Impact of the anchoring strength in the modal birefringence of the bandgap fiber studied in Fig. 3 for a PP configuration of the nematic material infiltrated in the lattice holes at $\beta\Lambda = 7$ for a defect-core radius of $r_c = 0.2\Lambda$.

$r_c = 0.2\Lambda$, $r = 0.3\Lambda$ at $\beta\Lambda = 7$, for instance, the birefringence varies from 1.25×10^{-2} at the strong to 2.03×10^{-2} at the weak-anchoring limit. It is clear that in the strong-anchoring limit, the birefringence is significantly reduced.

Although the above transition is related to the anchoring strength at the surface of the capillaries, it should be admissible to assume that it describes in an indicative manner the impact of any transition between the strong-anchoring limit and the uniform case as far as the bandgap fiber's properties are concerned. Given that light is not guided through the LC infiltrated cavities, the exact form of the director's pattern seems not to be of critical importance, since the birefringent effect is induced by a rather averaged effective contribution of the director pattern over the whole cross section. Thus, it should be also possible to dynamically control the modal birefringence values. Consider, for instance, the structure of Fig. 1, and assume that for $V_x = V_y = 0$, a PP pattern at the strong-anchoring limit is observed. By controlling the magnitude of the electric field, a continuous transition up to the quasi-uniform profile of Fig. 6(c) could be readily achieved, leading to a substantial birefringence tuning. Numerical simulations for the fiber studied in Fig. 8 $(r = 0.3\Lambda)$ predicted a birefringence value of 1.69×10^{-2} for a hard-anchoring strong-field $(R/\xi' = 15)$ case close to the limit of Fig. 6(c). This value is 16.8% lower compared to the one predicted for the fully uniform pattern of Fig. 6(b). The above calculation quantified the impact of an incomplete LC reorientation due to the anchoring effects on the modal birefringence for applied electric fields of high intensity. In a similar context, in the case where the ER pattern is exhibited for $V_x = V_y = 0$, the modal birefringence values could be tuned between zero values (modal degeneracy) up to a maximum value at the voltage, which ensures a transition close to the uniform profile.

III. Conclusion

PM and HB photonic bandgap fibers can be designed by infiltrating the cladding's holes of a conventional photonic bandgap fiber. The fiber's structure remains undisturbed, while light is still guided through a lower index defect core without entering the infiltrated capillaries. Thus, no extra issues such as scattering/absorption losses or material dispersion arise due to the presence of the nematic LC. Depending on the selection of the fiberglass, the nematic material, and the fiber's design parameters, the modal birefringence can be extensively adjusted. Birefringence values of up to 2×10^{-2} were numerically predicted for a common nematic compound such as E7. Finally, the possibility of dynamically controlling the fiber's dispersive properties via the application of an external electric field was also assessed, suggesting the operation of the fiber in a selective PM or tunable HB state.

References

[1] A. Bjarklev, J. Broeng, and A. S. Bjarklev, *Photonic Crystal Fibers*. Boston, MA: Kluwer, 2003.

[2] J. C. Knight, "Photonic crystal fibers," *Nature*, vol. 424, no. 6950, pp. 847–851, Aug. 2003.

[3] K. Tajima, J. Zhou, K. Nakajima, and K. Sato, "Ultralow loss and long length photonic crystal fiber," *J. Lightw. Technol.*, vol. 22, no. 1, pp. 7–10, Jan. 2004.

[4] H. Kubota, S. Kawanishi, S. Koyanagi, M. Tanaka, and S. Yamaguchi, "Absolutely single polarization photonic crystal fiber," *IEEE Photon. Technol. Lett.*, vol. 16, no. 1, pp. 182–184, Jan. 2004.

[5] J. Ju, W. Jin, and M. S. Demokan, "Design of single-polarization single-mode photonic crystal fiber at 1.30 and 1.55 μm," *J. Lightw. Technol.*, vol. 24, no. 2, pp. 825–830, Feb. 2006.

[6] T. P. Hansen, J. Broeng, S. E. B. Libori, E. Knudsen, A. Bjarklev, J. R. Jensen, and H. Simonsen, "Highly birefringent index-guiding photonic crystal fibers," *IEEE Photon. Technol. Lett.*, vol. 13, no. 6, pp. 588–590, Jun. 2001.

[7] T. Schreiber, F. Röser, O. Schmidt, J. Limpert, R. Iliew, F. Lederer, A. Petersson, C. Jacobsen, K. P. Hansen, J. Broeng, and A. Tünnermann, "Stress-induced single-polarization single-transverse mode photonic crystal fiber with low nonlinearity," *Opt. Express*, vol. 13, no. 19, pp. 7621–7630, Sep. 2005.

[8] K. Saitoh and M. Koshiba, "Photonic bandgap fibers with high birefringence," *IEEE Photon. Technol. Lett.*, vol. 14, no. 9, pp. 1291–1293, Sep. 2002.

[9] X. Chen, M.-J. Li, N. Venkataraman, M. T. Gallagher, W. A. Wood, A. M. Crowley, J. P. Carberry, L. A. Zenteno, and K. W. Koch, "Highly birefringent hollow-core photonic bandgap fiber," *Opt. Express*, vol. 12, no. 16, pp. 3888–3893, Aug. 2004.
[10] C. Kerbage and B. J. Eggleton, "Numerical analysis and experimental design of tunable birefringence in microstructured optical fiber," *Opt. Express*, vol. 10, no. 5, pp. 245–255, May 2002.
[11] H. Lim, A. Chong, and F. Wise, "Environmentally-stable femtosecond ytterbium fiber laser with birefringent photonic bandgap fiber," *Opt. Express*, vol. 13, no. 9, pp. 3460–3464, May 2005.
[12] M. Lehtonen, G. Genty, H. Ludvigsen, and M. Kaivola, "Supercontinuum generation in a highly birefringent microstructured fiber," *App. Phys. Lett.*, vol. 82, no. 14, pp. 2197–2199, Apr. 2003.
[13] A. Proulx, J.-M. Ménard, N. Hô, J. M. Laniel, R. Vallée, and C. Paré, "Intensity and polarization dependences of the supercontinuum generation in birefringent and highly nonlinear microstructured fibers," *Opt. Express*, vol. 11, no. 25, pp. 3338–3345, Dec. 2003.
[14] T. T. Larsen, A. Bjarklev, D. S. Hermann, and J. Broeng, "Optical devices based on liquid crystal photonic fibers," *Opt. Express*, vol. 11, no. 20, pp. 2589–2596, Oct. 2003.
[15] M. W. Haakestad, T. T. Alkeskjold, M. Nielsen, L. Scolari, J. Riishede, H. E. Engan, and A. Bjarklev, "Electrically tunable photonic bandgap guidance in a liquid-crystal-filled photonic crystal fiber," *IEEE Photon. Technol. Lett.*, vol. 17, no. 4, pp. 819–821, Apr. 2005.
[16] D. C. Zografopoulos, E. E. Kriezis, and T. D. Tsiboukis, "Photonic crystal-liquid crystal fibers for single-polarization or high-birefringence guidance," *Opt. Express*, vol. 14, no. 2, pp. 914–925, Jan. 2006.
[17] K. Nielsen, D. Noordegraaf, T. Sørensen, A. Bjarklev, and T. P. Hansen, "Selective filling of photonic crystal fibers," *J. Opt. A, Pure Appl. Opt.*, vol. 7, no. 8, pp. L13–L20, Aug. 2005.
[18] L. Xiao, W. Jin, M. S. Demokan, H. L. Ho, Y. L. Hoo, and C. Zhao, "Fabrication of selective injection microstructured optical fibers with a conventional fusion splicer," *Opt. Express*, vol. 13, no. 22, pp. 9014–9022, Oct. 2005.
[19] Y. Huang, Y. Xu, and A. Yariv, "Fabrication of functional microstructured optical fibers through a selective-filling technique," *Appl. Phys. Lett.*, vol. 85, no. 22, pp. 5182–5184, Nov. 2004.
[20] B. R. Acharya, K. W. Baldwin, J. A. Rogers, C. C. Huang, and R. Pindak, "In-fiber nematic liquid crystal optical modulator based on in-plane switching with microsecond response time," *Appl. Phys. Lett.*, vol. 81, no. 27, pp. 5243–5245, Dec. 2002.
[21] J. M. Pottage, D. M. Bird, T. D. Hedley, T. A. Birks, J. C. Knight, and P. S. J. Rusell, "Robust photonic band gaps for hollow core guidance in PCF made from high index glass," *Opt. Express*, vol. 11, no. 22, pp. 2854–2861, Nov. 2003.
[22] G. J. Pearce, J. M. Pottage, D. M. Bird, P. J. Roberts, J. C. Knight, and P. S. J. Russell, "Hollow-core PCF for guidance in the mid to far infrared," *Opt. Express*, vol. 13, no. 18, pp. 6937–6946, Sep. 2005.
[23] B. Bahadur, *Liquid Crystals: Applications and Uses*, vol. 1. Singapore: World Scientific, 1990.
[24] X. Feng, A. K. Mairaj, D. W. Hewak, and T. M. Monro, "Nonsilica glasses for holey fibers," *J. Lightw. Technol.*, vol. 23, no. 6, pp. 2046–2054, Jun. 2005.
[25] S. G. Johnson and J. D. Joannopoulos, *The MIT Photonic-Bands Package*. [Online]. Available: http://ab-initio.mit.edu/mpb/
[26] ——, "Block-iterative frequency-domain methods for Maxwell's equations in a planewave basis," *Opt. Express*, vol. 8, no. 3, pp. 173–190, Jan. 2001.
[27] A. P. Zhao, J. Juntunen, and A. V. Räisänen, "A generalized compact 2-d fdtd model for the analysis of guided modes of anisotropic waveguides with arbitrary tensor permittivity," *Microw. Opt. Technol. Lett.*, vol. 18, no. 1, pp. 17–23, 1998.
[28] C. O. Catanescu, S.-T. Wu, and L.-C. Chien, "Tailoring the physical properties of some high birefringence isothiocyanato-based liquid crystals," *Liq. Cryst.*, vol. 31, no. 4, pp. 541–555, Apr. 2004.
[29] J. Li, S.-T. Wu, S. Brugioni, R. Meucci, and S. Faetti, "Infrared refractive indices of liquid crystals," *J. Appl. Phys*, vol. 97, no. 7, p. 073501, Apr. 2005.
[30] G. P. Crawford, D. W. Allender, and J. W. Doane, "Surface elastic and molecular-anchoring properties of nematic liquid crystals confined to cylindrical cavities," *Phys. Rev. A*, vol. 45, no. 12, pp. 8693–8710, Jun. 1992.
[31] S. V. Burylov, "Equilibrium configuration of a nematic liquid crystal confined to a cylindrical cavity," *J. Exp. Theor. Phys.*, vol. 85, no. 5, pp. 873–886, Nov. 1997.
[32] S. Žumer and J. W. Doane, "Light scattering from a small nematic droplet," *Phys. Rev. A*, vol. 34, no. 4, pp. 3373–3385, Oct. 1986.
[33] J. F. Strömer, E. P. Raynes, and C. V. Brown, "Study of elastic constant ratios in nematic liquid crystals," *Appl. Phys. Lett*, vol. 88, no. 5, p. 051915, Jan. 2006.

Dimitrios C. Zografopoulos was born in Thessaloniki, Greece, in 1980. He received the Diploma degree in electrical and computer engineering from Aristotle University of Thessaloniki (AUTH) in 2003, where he is currently working toward the Ph.D. degree.

His research interests include computational electromagnetics, emphasizing the analysis and design of optical waveguides and photonic/liquid-crystal devices.

Emmanouil E. Kriezis (S'93–M'96) was born in Thessaloniki, Greece, in 1968. He received the Diploma degree in electrical engineering and the Doctorate degree from the Department of Electrical and Computer Engineering, Aristotle University of Thessaloniki (AUTH), in 1991 and 1996, respectively. His doctoral thesis focused on the development of full vector beam propagation methods for light-wave propagation in integrated optical devices.

In 1998, he joined the University of Oxford Department of Engineering Science, Oxford, U.K., initially as an EPSRC Postdoctoral Researcher. In September 2002, he was appointed as an Assistant Professor in optical and microwave communications with the Department of Electrical and Computer Engineering, AUTH. His research interests include methods of light-wave propagation, analysis of integrated optical devices, liquid-crystal devices, photonic crystals, and diffractive elements.

Dr. Kriezis is a member of the IEEE Lasers and Electro-Optics Society. In 2001, he was awarded the prestigious Royal Society University Research Fellowship to study light propagation in complex anisotropic media.

Theodoros D. Tsiboukis (M'91–SM'99) received the Diploma degree in electrical and mechanical engineering from the National Technical University of Athens, Athens, Greece, in 1971 and the Doctor Engineer degree from the Aristotle University of Thessaloniki (AUTH), Thessaloniki, Greece, in 1981.

From 1981 to 1982, he was with the Electrical Engineering Department, University of Southampton, Southampton, U.K., as a Senior Research Fellow. Since 1982, he has been working with the Department of Electrical and Computer Engineering (DECE), AUTH, where he is currently a Professor. His main research interests include electromagnetic-field analysis by energy methods, computational electromagnetics (FEM, BEM, vector finite elements, MoM, FDTD, ABCs), and inverse and EMC problems. He has authored or coauthored six books, more than 120 refereed journal articles, and more than 100 international conference papers.

Dr. Tsiboukis was the Guest Editor of a special issue of the *International Journal of Theoretical Electrotechnics* in 1996 and the Chairman of the local organizing committee of the 8th International Symposium on Theoretical Electrical Engineering in 1995. He has served in many administrative positions, including Director of the Division of Telecommunications with DECE in 1993–1998 and Chairman of the DECE in 1997–2001. He was awarded several distinctions and is a member of various societies, associations, chambers, and institutions.